Path Following with Disturbance Rejection for Inhomogeneous Formations with Underactuated Agents

D.J.W. Belleter and K.Y. Pettersen

***Abstract*— This paper considers straight-line path following for inhomogeneous formations with underactuated agents. The formation can be comprised of agents with different dynamics that are each affected by a different unknown environmental disturbance. Formation path following is achieved using a twofold strategy consisting of a guidance law to steer each vessel to a predefined path and a decentralised nonlinear formation control law utilising local information only to synchronise the agents position along the path such that a desired formation is achieved. The resulting closed-loop error dynamics consisting of the path-following error dynamics and formation error dynamics is analysed using theory for feedback-interconnected systems. The origin of the closed-loop error dynamics is shown to be uniformly globally asymptotically stable. The control strategy is validated with simulation results in a case study.**

I. Introduction

Multiagent control systems have been an active field of research in recent years. Multiagent operations have several advantages over conventional single agent operations. Using multiple agents allows tasks for single agents to be done in parallel making operations more time efficient. Moreover, multiple simpler agents can take over tasks of a more complex and costly single agent.

There has been a lot of research considering the control of multiple networked vehicles, see for instance [1]–[3] and the references therein. Formation control is an important aspect of cooperative control and has drawn attention for a large amount of applications, e.g. mobile robots [4], satellites [5], and marine vehicles [6].

Other works considering formation path-following of marine vehicles include [7]–[12]. In [7] coordinated path following in the presence of communication failures and time delays is considered for formations of underactuated vehicles without environmental disturbances. In [8] straight-line path following for formations of marine vehicles is considered, line of sight (LOS) guidance is used to make each vehicle converge to a desired path, whilst a formation control law synchronises the inter-agent distance to achieve a formation. The vessels in [8] are underactuated, but no environmental disturbances are considered. In the more recent work [9], formation control of underactuated vessels along closed orbits is considered but disturbances are not taken into account. Ocean current are considered in for instance [6], [10], however these works consider fully actuated marine vehicles. In [11], [12] formation control of underactuated vessels under the influence of constant disturbances is considered. Model uncertainties are also taken into account in [11], however only ultimate boundedness of the closed loop errors is achieved. The approach in [12] requires knowledge or estimation of the side-slip angle, while this is not necessary in the integral LOS guidance developed in [13] that is used in this work.

This work was partly supported by the Research Council of Norway through its Centres of Excellence funding scheme, project No. 223254 AMOS.

D.J.W. Belleter and K.Y. Pettersen are with the Centre for Autonomous Marine Operations and Systems (AMOS) and the Department of Engineering Cybernetics, Norwegian University of Science and Technology, NO7491 Trondheim, Norway {dennis.belleter,kristin.y.pettersen}@itk.ntnu.no.

A path-following control strategy for formations of underactuated marine vehicles in the presence of ocean currents is presented in [14]. The vehicles in [14] are controlled to a desired path using integral LOS guidance ([13], [15]) to reject the disturbance and a decentralised formation controller is used to synchronise the along-path position using only locally available information. However, in [14] it is assumed that the current for each vessel is the same, which is typically not the case if vessels are far apart or if one is shielding the other from the current. Moreover, the path following controller cannot be tuned considering individual vessel dynamics and limitations but should be the same for each vessel in the formation.

The class of systems and disturbances considered in this paper is the same as in [16]. However, [16] considers leader-follower synchronisation rather than mutual synchronisation as in this work. Moreover, the control strategy in [16] is trajectory independent while we here consider straight-line paths. Furthermore, the follower in [16] requires information about the planar position and velocity of the leader to synchronise its position, while in this work only the along path position of the other vehicle is required for synchronisation.

The main contribution in this work is to extend the work in [14] by removing the most limiting assumption. More, specifically, in [14] it is assumed that all the vessels are disturbed by the same current, which is necessary because the vessels are controlled to a constant desired relative velocity. In this work the vessels are controlled to a constant along-path velocity allowing for a vessel-specific relative velocity to reject the non-identical disturbances. Although the ocean current disturbances are allowed to be different for each vessel, they still have to be constant for each vessel to satisfy the modelling assumptions and conditions of the stability proof. Furthermore, it is an advantage of the new approach that different relative surge velocities also allow for vessel-specific tuning of the integral LOS guidance such that it can be tuned differently according to each vessel's limitations, dynamics, and dimensions. Furthermore the approach chosen in this paper allows for formations consisting of both fully actuated and underactuated agents, which is not the case in [14].

The paper is organised as follows. In Section II the dynamic for the agents is given, and the control goals and communication network is discussed. Section III introduced the guidance law and control system. The stability of the closed-loop system is investigated in Section IV. Section V presents a case study and Section VI gives some conclusions.

II. The Agents

This section presents the model used for the underactuated agents, the unknown environmental disturbance affecting the agents, the control goals, and the communication network between the agents. The formation path-following strategy is developed for a class of system described by a 3-DOF manoeuvring model and are moving in the horizontal plane. Examples of agents that are in this class of systems are underactuated autonomous surface vessels

(ASV) and underactuated autonomous underwater vehicles (AUV) moving in the horizontal plane. The proposed control strategy which combines adaptive path-following and formation control, can be extended to other classes of systems by considering a dynamic model, control scheme, and disturbances appropriate for that class of system.

A. The Vessel Model

In this work we consider ASVs or AUVs moving in the horizontal plane. The position and orientation of the vessels, $\boldsymbol{p}^i \triangleq [x, y, \psi]^T$, are described with respect to to an inertial frame, denoted by superscript i. The earth-fixed north-east-down frame is commonly used as inertial frame for marine vessels [17]. The linear and angular velocities of the vessels, $\boldsymbol{\nu} \triangleq [u, v, r]^T$, are expressed in a body-fixed reference frame, denoted b. Hence, the dynamics and kinematics of the vessel consist of the vessel's position and orientation, and its surge velocity u, sway velocity v, yaw rate r.

The environmental disturbance is an ocean current expressed in the inertial frame, it is denoted $\boldsymbol{V}_c$ and satisfies the following assumption.

Assumption 1: The ocean current, $\boldsymbol{V}_c \triangleq [V_x, V_y, 0]^T$, is assumed to be constant and irrotational with respect to the inertial frame. Furthermore it is bounded by $V_{\max}$ such that $\|\boldsymbol{V}_c\| = \sqrt{V_x^2 + V_y^2} \leq V_{\max}$.

For control purposes the model is expressed in terms of the relative velocity in the body-fixed reference frame, i.e. $\boldsymbol{\nu}_r \triangleq \boldsymbol{\nu} - \boldsymbol{\nu}_{cr} = [u_r, v_r, r]^T$. The ocean current velocity in the body-fixed frame $\boldsymbol{\nu}_{cr} \triangleq [u_{cr}, v_{cr}, 0]^T$, can be obtained by $\boldsymbol{\nu}_{cr} = \boldsymbol{R}^T(\psi)\boldsymbol{V}_c$, with $\boldsymbol{R}(\psi)$ denoting the rotation matrix from the body-fixed to the inertial reference frame

$$\boldsymbol{R}(\psi) \triangleq \begin{bmatrix} \cos(\psi) & -\sin(\psi) & 0 \\ \sin(\psi) & \cos(\psi) & 0 \\ 0 & 0 & 1 \end{bmatrix}. \tag{1}$$

Since the ocean current is irrotational, surface vessels, and also underwater vehicles moving in the horizontal plane, are described by the 3-DOF manoeuvring model from [17]:

$$\dot{\boldsymbol{p}}^i = \boldsymbol{R}(\psi)\boldsymbol{\nu}_r + [V_x, V_y, 0]^T \tag{2}$$

$$\boldsymbol{M}\dot{\boldsymbol{\nu}}_r + \boldsymbol{C}(\boldsymbol{\nu}_r)\boldsymbol{\nu}_r + \boldsymbol{D}\boldsymbol{\nu}_r = \boldsymbol{B}\boldsymbol{f}. \tag{3}$$

The vector $\boldsymbol{f} \triangleq [T_u, T_r]^T$ is the control input vector, containing the surge thrust T_u and the rudder angle T_r. The matrix $\boldsymbol{M} = \boldsymbol{M}^T > 0$ is the system inertia matrix including added mass, $\boldsymbol{C}$ is the Coriolis and centripetal matrix, $\boldsymbol{D}$ is the hydrodynamic damping matrix, and $\boldsymbol{B}$ is the actuator configuration matrix.

Assumption 2: We assume port-starboard symmetry.

Remark 1: Assumption 2 is to the authors' best knowledge satisfied for all commercial surface and underwater vessels.

The matrices $\boldsymbol{M}$, $\boldsymbol{D}$, and $\boldsymbol{B}$ are defined as

$$\boldsymbol{M} \triangleq \begin{bmatrix} m_{11} & 0 & 0 \\ 0 & m_{22} & m_{23} \\ 0 & m_{23} & m_{33} \end{bmatrix}, \boldsymbol{D} \triangleq \begin{bmatrix} d_{11} & 0 & 0 \\ 0 & d_{22} & d_{23} \\ 0 & d_{23} & d_{33} \end{bmatrix}, \boldsymbol{B} \triangleq \begin{bmatrix} b_{11} & 0 \\ 0 & b_{22} \\ 0 & b_{32} \end{bmatrix},$$

and $\boldsymbol{C}$ can be derived from $\boldsymbol{M}$ (See [17]). Since M is positive definite, and the damping is dissipative, the constant $d_{11}/m_{11} > 0$. For the special case of underwater vehicles moving in the horizontal plane, the matrices $\boldsymbol{M}$ and $\boldsymbol{D}$ will typically be diagonal.

Assumption 3: It is assumed the position of the body-fixed frame is chosen such that $\boldsymbol{M}^{-1}\boldsymbol{B}\boldsymbol{f} = [\tau_u, 0, \tau_r]^T$.

Remark 2: This is possible as long as the center of mass is located along the centreline of the vessel. Coordinate transformations for this translation can be found in [18].

The model can be written in component form as

$$\dot{x} = u_r\cos(\psi) - v_r\sin(\psi) + V_x, \tag{4a}$$

$$\dot{y} = u_r\sin(\psi) + v_r\cos(\psi) + V_y, \tag{4b}$$

$$\dot{\psi} = r, \tag{4c}$$

$$\dot{u}_r = F_{u_r}(v_r, r) - \tfrac{d_{11}}{m_{11}}u_r + \tau_u, \tag{4d}$$

$$\dot{v}_r = X(u_r)r + Y(u_r)v_r, \tag{4e}$$

$$\dot{r} = F_r(u_r, v_r, r) + \tau_r, \tag{4f}$$

which is clearly underactuated in sway. The definitions of F_{u_r}, $X(u_r)$, $Y(u_r)$, and F_r are given in Appendix I. Note that $X(u_r)$ and $Y(u_r)$ are bounded for bounded arguments and $Y(u_r)$ satisfies the following assumption.

Assumption 4: It is assumed that $Y(u_r)$ satisfies

$$Y(u_r) \leq -Y_{\min} < 0, \, \forall u_r \in [-V_{\max} - a, U_{\max}],$$

with a a parameter of the formation control law to be defined later and $U_{\max}$ the maximum attainable surge speed.

Remark 3: This assumption is satisfied for commercial vessels by design, since $Y(u_r) \geq 0$ would imply an undamped or nominally unstable vessel in the sway direction.

B. The Control Goals

The goal is to synchronise the position of n vessels along a predefined straight-line path $\mathcal{P}$ to achieve a desired formation. Hence, the control strategy is twofold in the sense that the vessels should individually converge to their respective desired path and synchronisation of the relative along-path position between the agents is required to achieve the desired formation. An example of a desired formation is given in Figure 1. The inertial frame is chosen such that its x-axis is aligned with the desired path, and consequently $\mathcal{P} \triangleq \{(x, y) \in \mathbb{R}^2 : y = 0\}$. The vessels should move along the path with a desired constant inertial frame velocity $\boldsymbol{v}_d^i = [\boldsymbol{v}_{d,x}^i, 0]^T$ with $\boldsymbol{v}_{d,x}^i > 0$ as illustrated in Figure 1. Note that this implies that vessels experiencing a different current $\boldsymbol{V}_c$ will have a different u_r and ψ_{ss} to achieve the same desired inertial frame velocity $\boldsymbol{v}_d^i$. The nonzero steady-state yaw angle ψ_{ss} is necessary to allow the underactuated vessels to side-slip. Side-slipping allows the underactuated vessels to stay on the path in the presence of currents. The desired position of the jth vessel in the formation is described by the distance to the path D_j and by a relative distance between agent i and j along the path d_{ji}. For the jth vessels this results in the control objectives:

$$\lim_{t\to\infty} y_j(t) - D_j = 0, \tag{5}$$

$$\lim_{t\to\infty} \psi_j(t) = \psi_{ss_j}, \quad \psi_{ss_j} \in \left(-\tfrac{\pi}{2}, \tfrac{\pi}{2}\right), \tag{6}$$

$$\lim_{t\to\infty} \dot{x}_j - \boldsymbol{v}_{d,x}^i = 0, \tag{7}$$

$$\lim_{t\to\infty} x_j(t) - x_i(t) - d_{ji} = 0, \tag{8}$$

for $j, i = 1, \ldots, n$. The control goals clearly show the twofold nature of the control strategy. Since (5) and (6) are related to path following, while (7) and (8) are aimed at achieving and maintaining a desired inter-vessel distance.

C. The Communication Network

Completion of control goal (8) requires synchronisation of the desired relative along-path position. For a vessels to determine its relative along-path position with respect to the other vessels communication is required. For surface vessels the along-path postion, x-position, can be obtained from GPS or AIS measurements [19]. For underwater vehicle acoustic transponders are required to facilitate communication. In this work the communication is described by algebraic graph theory (for more information see [20]).

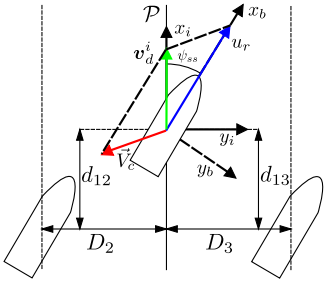

Fig. 1. The desired formation.

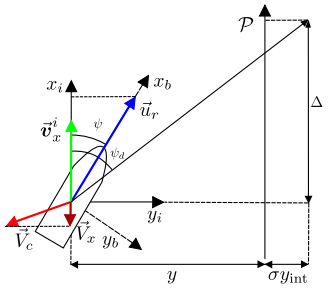

Fig. 2. Integral LOS guidance.

The communication topology is represented by a directed graph or digraph $\mathcal{G}(V, E)$ consisting of a set of vertices V representing the vessels and a set of edges E representing communication channels. More specifically, if there is information transfer from vertex v_i to v_j then the pair $(v_j, v_i) \in E$.

The neighbourhood $\mathcal{A}_j$ of v_j is the set of vertices $v_i \in V$ such that there is an edge from v_j to v_i. When controlling vessel j only the along-path position x_i of the vessels that are in its neighbourhood can be used, i.e. $i \in \mathcal{A}_j$. Using the graph representation we can make some definitions, based on [21], that are used in the analysis of the formation dynamics. A vertex $v_k \in V$ reachable from vertex $v_i \in V$ if there is a path from v_i to v_k. A vertex is globally reachable if it can be reached from every vertex in $\mathcal{G}(V, E)$. The graph is said to be strongly connected, if all vertices of $\mathcal{G}(V, E)$ are globally reachable.

III. The Control System

This section presents the heading controller and the velocity controller that are used to achieve the control goals of Subsection II-B. The heading controller consists of an integral LOS guidance law and a feedback linearising yaw rate controller. The velocity controller consists of a formation control law and a feedback linearising surge controller.

A. Heading Control

Each vessel uses an integral LOS guidance law, first introduced in [13], to calculate its desired heading angle. Integral LOS guidance allows the vessel to keep a nonzero yaw angle when to vehicle has converged to the path which allows for side-slipping [13]. The desired heading angle is calculated as

$$\psi_d \triangleq -\tan^{-1}\left(\tfrac{y+\sigma y_{\text{int}}}{\Delta}\right), \quad \Delta > 0, \tag{9a}$$

$$\dot{y}_{\text{int}} = \tfrac{\Delta y}{(y+\sigma y_{\text{int}})^2+\Delta^2}, \tag{9b}$$

with $\sigma > 0$ the integral gain and Δ the look-ahead distance. The integral LOS guidance scheme is illustrated in Figure 2.

Remark 4: The risk of integrator wind-up is reduced by the definition in (9b) which assures that the integral action is small when the cross-track error y is large.

To assure that ψ and r exponentially converge to ψ_d and $\dot{\psi}_d$ respectively the following feedback linearising PD controller is used to control the yaw rate

$$\tau_r = -F_r(u_r, v_r, r) + \ddot{\psi}_d - k_\psi(\psi - \psi_d) - k_r(r - \dot{\psi}_d). \tag{10}$$

B. Velocity Control

The velocity is controlled by controlling the relative surge velocity as can be seen from (4d). However, the velocity control goal (7) is formulated in terms in of the inertial frame velocity. Therefore the velocity error is translated from the inertial frame to the body-fixed frame using the transformation:

$$\begin{bmatrix} u_r - u_d \\ \tilde{v}_r \\ \tilde{\psi} \end{bmatrix} = \begin{bmatrix} \cos(\tilde{\psi}+\psi_d) & \sin(\tilde{\psi}+\psi_d) & 0 \\ -\sin(\tilde{\psi}+\psi_d) & \cos(\tilde{\psi}+\psi_d) & 0 \\ 0 & 0 & 1 \end{bmatrix} \begin{bmatrix} \dot{x} - \boldsymbol{v}_{d,x}^i \\ \dot{y} \\ \tilde{\psi} \end{bmatrix}. \tag{11}$$

Since this transformation is based on a rotation matrix, its inverse is well-defined in the entire state-space. Consequently, the transformation is a global diffeomorphism. The desired relative surge and sway velocity $u_d(t)$ and $v_d(t)$ can thus be calculated from the desired inertial frame velocity $\boldsymbol{v}_{d,x}^i$ from (7) using (11). Note that calculating the desired relative surge velocity from the velocity error in the inertial frame allows for a natural compensation of the x-component of the ocean current (see Figure 2) since $u_d(t)$ will implicitly contain a term to compensate the current. Moreover, since each vessel is controlled to $\boldsymbol{v}_d^i$, which is the desired velocity with respect to the same inertial frame, each vessel will have the same path-following velocity whilst compensating for a different current by having a different u_d and ψ_d.

Assumption 5: It is assumed that $V_{\max} < U_{\min} + a < u_d(t) < U_{\max} - a$ with $U_{\max} < U_M$, where U_M is the maximum attainable surge velocity of the vessel.

Remark 5: Assumption 5 requires that the vessel can achieve a relative surge speed higher than the sum of the maximum of the current and some additional freedom in the velocity used for the formation control. In general, Assumption 5 is easily satisfied since propulsion systems are designed to achieve much higher relative surge velocities than the velocity of the ocean current usually is. Furthermore note Assumption 5 is easily enforced by appropriate saturation of the desired relative surge velocity $u_d(t)$ calculated from (11).

Remark 6: Note that for underactuated vessels only u_d calculated from (11) is necessary for control purposes, since the integral LOS guidance will assure that the current is compensated and that control goal (7) is achieved simultaneously. For fully actuated vessels, not utilising integral LOS guidance, a desired sway velocity v_d could also be calculated from (11) to achieve the same result.

Remark 7: Note that even though $u_d(t)$ is time-varying in the transient behaviour it will settle at a constant value u_{rd} which size is dependent on the desired inertial frame velocity and the magnitude and direction of the current. Unlike in [14] where it was controlled to the same constant value U_{rd} for each vessel and hence not allowing a different Δ, ψ_{ss}, and $\boldsymbol{V}_c$ for each vessel. Note however, that this extra freedom comes at the expense of the requirement of measurements of the inertial frame velocities $\dot{x}$ and $\dot{y}$. These can be obtained from GPS for ASVs or acoustic transponders for AUVs.

To achieve synchronisation of the relative along-path position a formation control term is added to the desired relative surge speed to obtain the control velocity assignment for the jth vessel

$$u_{c_j} = u_{d_j}(t) - g\Big(\sum_{i \in \mathcal{A}_j} (x_j - x_i - d_{ji})\Big) \tag{12}$$

with $g(x) : \mathbb{R} \to \mathbb{R}$ a continuously differentiable saturation-like function that satisfies

$$\begin{aligned} -a \le g(x) \le a, \quad \forall x \in \mathbb{R}, \quad g(0) = 0, \\ 0 < g'(x) \le \mu, \forall x \in \mathbb{R}, \quad g'(x) \triangleq dg/dx \end{aligned} \tag{13}$$

where a is the parameter from Assumptions 4 and 5, and $\mu > 0$ is an arbitrary constant. This also implies that the function $g(x)$ should be a sector function belonging to the sector $[0, \mu]$. A suitable choice for $g(x)$ is for example

$$g(x) \triangleq \tfrac{2a}{\pi} \tan^{-1}(x). \tag{14}$$

We want to make $u_{r_j}(t)$ track u_{c_j}. From (12) we see that when the formation is reached such that the second term is zero, then if $u_{r_j}(t)$ tracks u_{c_j} this implies that $u_{r_j}(t)$ tracks $u_{d_j}(t)$. It is implied by (11) that controlling $u_{r_j}(t)$ to track u_{d_j} implies controlling $\dot{x}$ to the desired value $\boldsymbol{v}^i_{d,x}$ and thus achieving control goal (7).

To make $u_{r_j}(t)$ track u_{c_j} the following feedback linearising P controller is applied to (4d) (omitting the vessel-specific subscript):

$$\tau_u = -F_{u_r}(v_r, r) + \tfrac{d_{11}}{m_{11}} u_c + \dot{u}_c - k_{u_r}(u_r - u_c), \tag{15}$$

with $k_{u_r} > 0$ a constant gain. As in [15], part of the damping is not cancelled to guarantee some robustness with respect to model uncertainties.

C. Tracking Errors

To analyse the tracking errors of the heading and velocity controllers we introduce the vector $\boldsymbol{\xi} \triangleq [\tilde{u}_r, \tilde{\psi}, \tilde{r}]^T$, with the tracking errors $\tilde{u}_r \triangleq u_r - u_c$, $\tilde{\psi} \triangleq \psi - \psi_d$, and $\tilde{r} \triangleq r - \dot{\psi}_d$. The closed-loop tracking errors can be analysed by substituting the controllers (10) and (15) in the model (4) resulting in:

$$\dot{\boldsymbol{\xi}} = \begin{bmatrix} -k_{u_r} - \frac{d_{11}}{m_{11}} & 0 & 0 \\ 0 & 0 & 1 \\ 0 & -k_\psi & -k_r \end{bmatrix} \boldsymbol{\xi} \triangleq \Sigma \boldsymbol{\xi}. \tag{16}$$

The system (16) is linear and time-invariant and k_{u_r}, k_ψ, k_r, and d_{11}/m_{11} are strictly positive. Consequently, Σ is Hurwitz and the origin of (16) is uniformly globally exponentially stable (UGES).

Using the notation

$$X^{\max_j} \triangleq \max_{u_{c_j} \in [U_{\min}, U_{\max}]} |X_j(u_{c_j})| \tag{17}$$

$$Y^{\min_j} \triangleq \min_{u_{c_j} \in [U_{\min}, U_{\max}]} |Y_j(u_{c_j})| \tag{18}$$

the main result can then be formulated as follows.

Theorem 1: Consider a formation of n vessels described by (4). Suppose that u_d is continuously differentiable, Assumptions 1-5 are satisfied, and the communication graph contains at least one globally reachable vertex. If the look-ahead distance Δ and the integral gain σ satisfy the conditions

$$\Delta_j > \frac{|X_{\max_j}|}{|Y_{\min_j}|} \left[\frac{5}{4} \frac{U_{\max_j} + V_{\max_j} + \sigma_j}{U_{\min_j} - V_{\max_j} - \sigma_j} + 1 \right], \tag{19}$$

$$0 < \sigma_j < U_{\min_j} - V_{\max_j}, \tag{20}$$

for $j = 1, \ldots, n$, then the controllers (9-10), (15), guarantee achievement of the control goals (5)-(8).

Proof: The proof for this theorem is provided by the closed loop analysis of Section IV. ∎

IV. The Closed-Loop Dynamics

In this section we consider the complete closed-loop dynamics (4), (9-10), (15). This can be split into two parts. One part consists of the path following error dynamics for each vessel. The other part consists of the along-path or formation error dynamics. These two parts are then combined in a feedback-interconnected cascades system to show stability of the total closed-loop error dynamics.

A. Path Following Error Dynamics

In this subsection we consider the path-following error dynamics of a single vessel and therefore omit the vessel specific subscript j. The path following dynamics consist the dynamics of the cross-track error y, the integral state y_{int}, and the underactuated sway dynamics resulting in

$$\dot{y}_{\text{int}} = \tfrac{\Delta y}{(y + \sigma y_{\text{int}})^2 + \Delta^2} \tag{21}$$

$$\dot{y} = (\tilde{u}_r + u_c)\sin(\tilde{\psi} + \psi_d) + v_r \cos(\tilde{\psi} + \psi_d) + V_y \tag{22}$$

$$\dot{v}_r = X(\tilde{u}_r + u_c)(\dot{\tilde{\psi}} + \dot{\psi}_d) + Y(\tilde{u}_r + u_c) v_r. \tag{23}$$

To formulate the path-following error dynamics the equilibrium is moved to the origin using the definitions $e_1 \triangleq y_{\text{int}} - y^{\text{eq}}_{\text{int}}$ and $e_2 \triangleq (y - D_j) + \sigma e_1$ where

$$y^{\text{eq}}_{\text{int}} = \tfrac{\Delta}{\sigma} \tfrac{V_y}{\sqrt{u^2_{rd} - V^2_y}}, \quad y^{\text{eq}} = D_j, \quad v^{\text{eq}}_r = 0. \tag{24}$$

with u_{rd} the equilibrium relative velocity from Remark 7. These substitutions and factorizing with respect to (16) leads to the cascaded system

$$[\dot{e}_1, \dot{e}_2, \dot{v}_r]^T = \boldsymbol{A}[e_1, e_2, v_r]^T + \boldsymbol{B} f(e_2) + \boldsymbol{C} p(x) - \boldsymbol{H}_y \boldsymbol{\xi} \tag{25a}$$

$$\dot{\boldsymbol{\xi}} = \Sigma \boldsymbol{\xi}. \tag{25b}$$

with $\boldsymbol{A}$ as in (26) and $\boldsymbol{B}$, $\boldsymbol{C}$, and $\boldsymbol{H}$ defined as:

$$\boldsymbol{B}(e_2) \triangleq \begin{bmatrix} 0 & V_y & -\frac{\Delta X^{u_c} V_y}{(e_2 + \sigma y^{\text{eq}}_{\text{int}})^2 + \Delta^2} \end{bmatrix}^T, \tag{27}$$

$$\boldsymbol{C}(e_2) \triangleq \begin{bmatrix} 0 & \frac{\sigma y^{\text{eq}}_{\text{int}}}{(e_2 + \sigma y^{\text{eq}}_{\text{int}})^2 + \Delta^2} & \frac{\Delta X^{u_c} \sigma y^{\text{eq}}_{\text{int}}}{\left((e_2 + \sigma y^{\text{eq}}_{\text{int}})^2 + \Delta^2\right)^{3/2}} \end{bmatrix}^T, \tag{28}$$

$$\boldsymbol{H}_y(y, y_{\text{int}}, \psi_d, v_r, \boldsymbol{\xi}) \triangleq \begin{bmatrix} 0 & 0 \\ 1 & 0 \\ -\frac{\Delta X(\tilde{u}_r + u_c)}{(e_2 + \sigma y^{\text{eq}}_{\text{int}})^2 + \Delta^2} & 1 \end{bmatrix} \begin{bmatrix} \boldsymbol{h}_y^T \\ \boldsymbol{h}_{v_r}^T \end{bmatrix}, \tag{29}$$

with $\boldsymbol{h}_y^T$ and $\boldsymbol{h}_{v_r}^T$ defined in Appendix I,

$$f(e_2) = 1 - \frac{\sqrt{(\sigma y^{\text{eq}}_{\text{int}})^2 + \Delta^2}}{\sqrt{(e_2 + \sigma y^{\text{eq}}_{\text{int}})^2 + \Delta^2}}, \tag{30}$$

and $p(x) \triangleq u_c - u_{rd}$, which is the difference between the control velocity (12) and the equilibrium relative surge velocity, which is a function of x since u_c contains $g(x)$.

Remark 8: Note that the term $\boldsymbol{C}p(x)$ is a result of the combination of integral action/adaptation and formation control. Having only one of these features, as in [15] and [8], this term would be zero. In [14] this term is simply given by $\boldsymbol{C}g(x)$, since the desired velocity is constant except for the formation term $g(x)$ from (13).

Note that $f(e_2)$ satisfies the following bound:

$$|f(e_2)| \leq \frac{|e_2|}{\sqrt{(e_2 + \sigma y^{\text{eq}}_{\text{int}})^2 + \Delta^2}} \tag{31}$$

and that $\boldsymbol{H}_y \boldsymbol{\xi}$ contains the terms vanishing at $\boldsymbol{\xi} = \boldsymbol{0}$.

B. Formation Control Dynamics

The formation dynamics consists of the along-path dynamics of the vessels. The formulation of the formation dynamics will follow along the lines of that in [8] and [14], but with the new velocity assignment. The along-path dynamics are given by

$$\dot{x} = u_r \cos(\psi) - v_r \sin(\psi) + V_x. \tag{32}$$

Considering $u_r = \tilde{u}_r + u_c$, $\psi = \tilde{\psi} + \psi_d$, $\psi_d = \psi_{ss} + \psi_t$ where ψ_{ss} is the steady-state path-following angle (see Figure 1) and ψ_t a transient part that disappears when $e_2 = 0$, and $u_c = u_d - g(x)$, with $g(x)$ defined as in (13) results in

$$\dot{x} = u^i_x(t) - g(x)\cos(\psi_{ss}) + \boldsymbol{h}_x^T(\boldsymbol{\zeta}, x)\boldsymbol{\zeta}. \tag{33}$$

where $u_d(t)\cos\psi + V_x$ is replaced by its projection on the x-axis $u^i_x(t)$ and $\boldsymbol{h}_x^T \triangleq [h_{x,1}, \ldots, h_{x,6}]^T$ is given by

$$\begin{aligned} h_{x,1} &= \cos(\tilde{\psi} + \psi_d) \\ h_{x,2} &= g(x)\left[\tfrac{\sin(\tilde{\psi})}{\tilde{\psi}}\sin(\psi_d) - \tfrac{\cos(\tilde{\psi}) - 1}{\tilde{\psi}}\cos(\psi_d)\right] \\ h_{x,5} &= g(x)\left[\tfrac{\sin(\psi_t)}{e_2}\sin(\psi_{ss}) - \tfrac{\cos(\psi_t) - 1}{e_2}\cos(\psi_{ss})\right] \\ h_{x,3} &= h_{x,4} = 0;\ h_{x,6} = \sin(\tilde{\psi} + \psi_d). \end{aligned} \tag{34}$$

$$\boldsymbol{A}(e_2) \triangleq \begin{bmatrix} -\frac{\sigma\Delta}{(e_2+\sigma y_{\text{int}}^{\text{eq}})^2+\Delta^2} & \frac{\Delta}{(e_2+\sigma y_{\text{int}}^{\text{eq}})^2+\Delta^2} & 0 \\ -\frac{\sigma^2\Delta}{(e_2+\sigma y_{\text{int}}^{\text{eq}})^2+\Delta^2} & \left(\frac{\sigma\Delta}{(e_2+\sigma y_{\text{int}}^{\text{eq}})^2+\Delta^2}-\frac{u_c}{\sqrt{(e_2+\sigma y_{\text{int}}^{\text{eq}})^2+\Delta^2}}\right) & \frac{\Delta}{\sqrt{(e_2+\sigma y_{\text{int}}^{\text{eq}})^2+\Delta^2}} \\ \frac{\sigma^2\Delta^2 X^{u_c}}{((e_2+\sigma y_{\text{int}}^{\text{eq}})^2+\Delta^2)^2} & \left(\frac{u_c\Delta X^{u_c}}{((e_2+\sigma y_{\text{int}}^{\text{eq}})^2+\Delta^2)^{3/2}}-\frac{\sigma\Delta^2 X^{u_c}}{((e_2+\sigma y_{\text{int}}^{\text{eq}})^2+\Delta^2)^2}\right) & \left(Y^{u_c}-\frac{\Delta^2 X^{u_c}}{((e_2+\sigma y_{\text{int}}^{\text{eq}})^2+\Delta^2)^{3/2}}\right) \end{bmatrix} \tag{26}$$

Considering (33) in the context of a formation we can write

$$\dot{x}_j = u_x^i(t) - g\Big(\sum_{i\in\mathcal{A}_j}(x_j - x_i - d_{ji})\Big)\cos(\psi_{ss_j}) + \boldsymbol{h}_{x_j}^T\boldsymbol{\zeta}_j \tag{35}$$

with $j = 1,\ldots,n$. As in [8] and [14] a change of coordinates can be done where $\theta_j \triangleq x_j - d_j - \int_{t_0}^{t} u_x^i(s)ds$ for $j = 1,\ldots,n$ where d_j is such that $d_j - d_i = d_{ji}$, for $j,i = 1,\ldots,n$. This results in

$$\dot{\theta}_j = -g\Big(\sum_{i\in\mathcal{A}_j}(\theta_j - \theta_i)\Big)\cos(\psi_{ss_j}) + \boldsymbol{h}_{x_j}^T(\boldsymbol{\zeta}_j,\theta)\boldsymbol{\zeta}_j, \tag{36}$$

for $j = 1,\ldots,n$. It can be verified that $\theta_j - \theta_i = 0\ \forall\ i,j = 1,\ldots,n$ implies that (8) is achieved. This in turn implies that u_r converges to u_d which assures control goal (7) is achieved. Hence, it suffices to analyse (36) to prove achievement of both (7) and (8).

We now write the system in vector form by defining the aggregate state $\boldsymbol{\theta} \triangleq [\theta_1,\ldots,\theta_n]^T$, the aggregate function $\boldsymbol{g}(\boldsymbol{x}) \triangleq [g(x_1),\ldots,g(x_n)]^T$, and the aggregate matrices $\boldsymbol{\Lambda} \triangleq [\mathbf{diag}\{\cos(\psi_{ss_1}),\ldots,\cos(\psi_{ss_n})\}]$, $\boldsymbol{\zeta} \triangleq [\boldsymbol{\zeta}_1^T,\ldots,\boldsymbol{\zeta}_n^T]^T$, and $\boldsymbol{H}_x \triangleq [\boldsymbol{h}_{x_1},\ldots,\boldsymbol{h}_{x_n}]^T$. Such that (36) can be written as

$$\dot{\boldsymbol{\theta}} = -\boldsymbol{\Lambda}\boldsymbol{g}(\boldsymbol{L}\boldsymbol{\theta}) + \boldsymbol{H}_x(\boldsymbol{\zeta},\boldsymbol{\theta})\boldsymbol{\zeta} \tag{37}$$

where the $\boldsymbol{L}$ is the Laplacian matrix of the graph $\mathcal{G}$ with elements:

$$l_{ji} \triangleq \begin{cases} \delta_j & \text{if } j = i \\ -1, & \text{if } j \neq i\ \wedge\ (j,i)\in E,\ j,i = 1,\ldots,n \\ 0, & \text{otherwise} \end{cases} \tag{38}$$

with δ_j the number of outgoing edges from v_j. By definition the Laplacian has one or more eigenvalues at zero with the vector of all ones as eigenvector. If the graph is stronlgy connected -i.e. it has n globally reachable vertices- then the zero eigenvalue is simple and $\boldsymbol{L}$ is symmetric and positive semi-definite (see [20], [21]).

Remark 9: Although the system equation has differences with respect to the velocity assignment compared to [14] by proper substitution the structure of (37) is now equivalent to the system considered in [14].

As stated in [8] the consensus properties of the along-path dynamics cannot be determined by simply analysing its stability properties, since it can have multiple equilibria depending on the network topology. Therefore, a coordinate transform is proposed in [8, Lemma 2] which can also be derived for system equation (37).

Lemma 1 ([8, Lemma 2]): Consider system (37). Under the condition of Theorem 1 there exists a coordinate transformation $\boldsymbol{\phi} \triangleq \boldsymbol{T}\boldsymbol{\theta}$, $\boldsymbol{T} \in \mathbb{R}^{(n-1)\times n}$, such that the following holds:

1) $\boldsymbol{\phi} = \mathbf{0}$ implies that $\theta_1 = \ldots = \theta_n$;
2) the dynamics of $\boldsymbol{\phi}$ are of the form

$$\dot{\boldsymbol{\phi}} = \boldsymbol{f}(\boldsymbol{\phi}) + \boldsymbol{G}(\boldsymbol{\zeta},\boldsymbol{\phi})\boldsymbol{\zeta} \tag{39}$$

with $\boldsymbol{G}(\boldsymbol{\zeta},\boldsymbol{\phi})$ globally bounded, uniformly in $\boldsymbol{\zeta}$ and $\boldsymbol{\phi}$;
3) $\dot{\boldsymbol{\phi}} = \boldsymbol{f}(\boldsymbol{\phi})$ is UGAS with positive definite and radially unbounded Lyapunov function $V = V(\boldsymbol{\phi})$ satisfying

$$\frac{\partial V}{\partial \boldsymbol{\phi}}(\boldsymbol{\phi})\boldsymbol{f}(\boldsymbol{\phi}) \leq -W(\boldsymbol{\phi}) < 0,\ \forall \boldsymbol{\phi} \in \mathbb{R}^{n-1}\setminus\{\mathbf{0}\} \tag{40}$$

$$\left\|\frac{\partial V}{\partial \boldsymbol{\phi}}(\boldsymbol{\phi})\right\| \leq C_1,\ \forall \boldsymbol{\phi} \in \mathbb{R}^{n-1}. \tag{41}$$

Proof: The proof for the case considered here is equivalent to that in [14]. The only difference is that the perturbing term $\boldsymbol{G}(\boldsymbol{\zeta},\boldsymbol{\phi})$ is different, however it is trivial to show that $\boldsymbol{G}(\boldsymbol{\zeta},\boldsymbol{\phi})$ satisfies Condition 2) of the lemma. The proof is therefore omitted in favour of the resulting transformation. The transformation is based on a partitioning of the Laplacian:

$$\boldsymbol{L} = \begin{bmatrix} \boldsymbol{L}_1 & \boldsymbol{L}_2 \\ \mathbf{0} & \boldsymbol{M}_3\boldsymbol{M}_3^T \end{bmatrix} \tag{42}$$

resulting in the coordinate transformation:

$$\boldsymbol{\phi} \triangleq \begin{bmatrix} \boldsymbol{L}_1 & \boldsymbol{L}_2 \\ \mathbf{0} & \boldsymbol{M}_3^T \end{bmatrix}\boldsymbol{\theta} \triangleq \boldsymbol{T}\boldsymbol{\theta}. \tag{43}$$

Applying this coordinate transform results in

$$\dot{\boldsymbol{\phi}} = \begin{bmatrix} -\boldsymbol{L}_1\boldsymbol{\Lambda}_1\boldsymbol{g}_1(\boldsymbol{\phi}_1) - \boldsymbol{L}_2\boldsymbol{\Lambda}_2\boldsymbol{g}_2(\boldsymbol{\kappa}) \\ -\boldsymbol{M}_3^T\boldsymbol{\Lambda}_2\boldsymbol{g}_2(\boldsymbol{\kappa}) \end{bmatrix} + \boldsymbol{T}\boldsymbol{H}_x(\boldsymbol{\zeta},\boldsymbol{\theta})\boldsymbol{\zeta} \tag{44}$$

$$\triangleq \boldsymbol{f}(\boldsymbol{\phi}) + \boldsymbol{G}(\boldsymbol{\zeta},\boldsymbol{\theta})\boldsymbol{\zeta} \tag{45}$$

where $\boldsymbol{\phi} = [\boldsymbol{\phi}_1^T,\boldsymbol{\phi}_2^T]^T$, with $\boldsymbol{\phi}_1 \in \mathbb{R}^{n-r}$ and $\phi_2 \in \mathbb{R}^r$ where r satisfying $1 \leq r < n$ is the number of globally reachable vertices, and we defined $\boldsymbol{\kappa} \triangleq \boldsymbol{M}_3\boldsymbol{\phi}_2$ to simplify notation. Moreover, using (34) it is straightforward to verify that $\boldsymbol{G}(\boldsymbol{\zeta},\boldsymbol{\phi}) \triangleq \boldsymbol{T}\boldsymbol{H}_x(\boldsymbol{\zeta},\boldsymbol{\phi})$ is globally bounded in its arguments. ■

C. Closed-Loop Stability

The proof of closed-loop stability will follow along the lines of that in [14], but the bounds and conditions in the proof are different due to the new velocity assignment. To assess the closed-loop stability of the combined path-following error and formation dynamics we consider the cascaded system:

$$\dot{\boldsymbol{\phi}} = \boldsymbol{f}(\boldsymbol{\phi}) + \boldsymbol{G}(\boldsymbol{\zeta},\boldsymbol{\phi})\boldsymbol{\zeta} \tag{46a}$$

$$[\dot{e}_1,\dot{e}_2,\dot{v}_r]^T = \boldsymbol{A}[e_1,e_2,v_r]^T + \boldsymbol{B}f(e_2) + \boldsymbol{C}p(x) - \boldsymbol{H}_y\boldsymbol{\xi} \tag{46b}$$

$$\dot{\boldsymbol{\xi}} = \Sigma\boldsymbol{\xi}. \tag{46c}$$

Remark 10: Note that by a slight abuse of notation (46b) contains $p(x)$ instead of $p(\boldsymbol{\phi})$ and that the cross-track error system is in a non-aggregate form. This is done to make the analysis more clear, since path following is considered for individual vessels, while the along-path dynamics (46a) considers multiple vessels.

Remark 11: As noted in [14], (46) is a feedback-interconnected system and not a classical cascade since (46b) contains the term $p(x)$ which depends on the along-path variable x because it is induced by $g(x)$ from the velocity assignment (12). As stated in Remark 8 this is a consequence of the combined integral action and formation control

Feedback-interconnected systems can be analysed as cascade-interconnected system using a technique called 'breaking the loop', as introduced in [22]. In [22] it is shown how a system of the form:

$$\dot{x}_1 = f_1(t,x_1) + g(t,x_1,x_2) \tag{47a}$$

$$\dot{x}_2 = f_2(t,x_1,x_2) \tag{47b}$$

can be analysed as a cascaded system of the form

$$\dot{\xi}_1 = f_1(t,\xi_1) + g(t,\xi_1,\xi_2)\xi_2 \tag{48a}$$

$$\dot{\xi}_2 = f_2(t, x_1(t), \xi_2) = \tilde{f}_2(t, \xi_2) \tag{48b}$$

where $f_2(t, x_1(t), \xi_2)$ depends on the *parameter* x_1, with $x_1(t)$ denoting solutions of (47a).

As discussed in [14] for the system (46) the nominal term $f_1(t, \xi_1) = f_1(t, x)$ is of the same order with respect to x as the perturbing term $g(t, \xi_1, \xi_2)\xi_2 = g(t, x, \boldsymbol{\zeta})\zeta$. Therefore the following conditions are given in [22] for UGAS of the origin of (46)

1) $x_1 = 0$ is a UGAS equilibrium for $\dot{x}_1 = f_1(t, x_1)$.
2) The solutions of (46) are uniformly globally bounded.

Condition 1) translates to the closed-loop system (46) satisfying the following condition:

Condition 1: $\boldsymbol{\phi} = 0$ is a UGAS equilibrium for $\dot{\boldsymbol{\phi}} = \boldsymbol{f}(\boldsymbol{\phi})$.

Condition 1 is verified by the proof of claim 3) from Lemma 1.

Verifying condition 2) requires satisfying the following subconditions

Condition 2a: There exists a $\mathcal{C}^1$ positive definite radially unbounded function $\tilde{V} : \mathbb{R} \times \mathbb{R}^{n_1} \to \mathbb{R}_{\geq 0}, \alpha_1 \in \mathcal{K}_\infty$ and continuous non-decreasing functions $\alpha_4, \alpha_4' : \mathbb{R}_{\geq 0} \times \mathbb{R} \to \mathbb{R}_{\geq 0}$ such that

$$\tilde{V}(t, x_1) \geq \alpha_1(|x_1|) \tag{49}$$

and that,

$$\dot{\tilde{V}}_{(46a)}(t, x_1) \leq \alpha_4(|x_1|)\alpha_4'(|x_2|); \tag{50}$$

$$\int_a^\infty \frac{\mathrm{d}\tilde{v}}{\alpha_4(\alpha_1^{-1}(\tilde{v}))} = \infty \tag{51}$$

Condition 2a can be verified using the function

$$\tilde{V}_{(46a)}(\boldsymbol{\phi}) = \tfrac{1}{2}\boldsymbol{\phi}^2 \tag{52}$$

which is clearly $\mathcal{K}_\infty$, satisfying (49). From (52) is follows that

$$\dot{\tilde{V}}_{(46a)}(\boldsymbol{\phi}) \triangleq \frac{\partial \tilde{V}}{\partial t} + \frac{\partial \tilde{V}}{\partial \boldsymbol{\phi}}[\boldsymbol{f}(\boldsymbol{\phi}) + \boldsymbol{G}(\boldsymbol{\zeta}, \boldsymbol{\phi})\boldsymbol{\zeta}] = \boldsymbol{\phi}\dot{\boldsymbol{\phi}}. \tag{53}$$

Using (44) and (34) it can be verified that functions

$$\alpha_4(|\boldsymbol{\phi}|) \triangleq |\boldsymbol{\phi}|^T \tag{54}$$

$$\alpha_4'(|\boldsymbol{\zeta}|) \triangleq |\boldsymbol{T}| \begin{bmatrix} |\tilde{u}_{r_1}|+8a+|v_{r_1}| \\ \vdots \\ |\tilde{u}_{r_n}|+8a+|v_{r_n}| \end{bmatrix} \tag{55}$$

satisfy the inequality

$$\dot{\tilde{V}}_{(46a)}(\boldsymbol{\phi}) \leq \alpha_4(|\boldsymbol{\phi}|)\alpha_4'(|\boldsymbol{\zeta}|)$$

with $\alpha_4, \alpha_4' : \mathbb{R}_{\geq 0} \times \mathbb{R} \to \mathbb{R}_{\geq 0}$ continuous and non-decreasing with respect to their arguments.

To verify that (51) holds, note that $\alpha_1^{-1}(\tilde{v}) = \sqrt{2\tilde{v}}$ and consequently it holds that

$$\int_a^\infty \frac{\mathrm{d}\tilde{v}}{\alpha_4(\alpha_1^{-1}(\tilde{v}))} = \int_a^\infty \frac{\mathrm{d}\tilde{v}}{\sqrt{2\tilde{v}}} = \infty.$$

Condition 2b: We dispose of a $\mathcal{C}^1$ function $V : \mathbb{R} \times \mathbb{R}^{n_1} \to \mathbb{R}_{\geq 0}$, $\alpha_1, \alpha_2 \in \mathcal{K}_\infty$, and a positive semidefinite function W such that

$$\alpha_1(|x_1|) \leq V(t, x_1) \leq \alpha_2(|x_1|) \tag{56}$$

$$\frac{\partial V}{\partial t} + \frac{\partial V}{\partial x_1} f_1(t, x_1) \leq -W(x_1) \tag{57}$$

for all $t \in [t_o, t_{\max})$ and all $x_1 \in \mathbb{R}^{n_1}$.

Condition 2b holds as a direct consequence of Condition 1 being satisfied.

Condition 2c: There exists $\beta \in \mathcal{KL}$ such that the solutions $x_2(t, t_o, x_{2o}, x_1)$ of $\dot{x}_2 = \tilde{f}_2(t, x_2)$ satisfy

$$|x_2(t, t_o, x_{2o}, x_1)| \leq \beta(|x_{2o}|, t - t_o) \quad \forall t \in [t_o, t_{\max}). \tag{58}$$

Condition 2c can be verified using the stability proof from [15]. In [15] the origin of the path-following error dynamics (46b) is shown to be stable for constant reference velocities satisfying Assumption 5. It should be noted that $|x_2(t, t_o, x_{2o}, x_1)|$ represents the solutions of (47b) for fixed values of the parameter x_1, i.e. solutions of the path-following error dynamics (46b) for fixed values of the coordination error $\boldsymbol{\phi}$ and hence fixed values of the formation term $g(x)$ of the velocity. Therefore, to verify that Condition 2c holds we only need to show that the desired velocity $u_d(t)$ derived from the transformation (11) can vary when converging on the path, but is constant when on the path. As mentioned the path-following error dynamics (25) converge to the origin for any velocity satisfying Assumption 5, which is something that is assured by the velocity transformation (11). By substitution of $\dot{x}$ and $\dot{y}$ in the velocity transformation, it can be verified that $u_d(t)$ is given by

$$u_d(t) = (\boldsymbol{v}_{d,x}^i - V_x)\cos(\psi_d) - V_y \sin(\psi_d), \tag{59}$$

which shows that the desired velocity is a function of the desired heading angle from the integral LOS guidance law (9). The integral LOS guidance law converges to a constant steady-state angle, $\psi_d \equiv \psi_{ss}$, while the vessel converges to the path. Consequently, the relative surge velocity also converges to a constant relative relative surge velocity given by

$$u_{rd} = (\boldsymbol{v}_{d,x}^i - V_x)\cos(\psi_{ss}) - V_y \sin(\psi_{ss}), \tag{60}$$

and hence the velocity is no longer adapted when the vessel has converged to the path. The resulting velocity assignment is given in Figure 3. It can be verified that (60) is the only possible solution for the velocity by realising that the steady-state angle is assigned by the integral LOS guidance law such that V_y is compensated, and using this angle the desired velocity is calculated such that the path is followed with $\boldsymbol{v}_{d,x}^i$. Therefore, the desired heading and desired relative surge velocity together assure that (24) is a unique equilibrium of the path-following strategy. Summarising, we know that the the integral LOS guidance law assures convergence to the path and the equilibrium on the path is unique and invariant when using the velocity transformation (11).

Consequently, the stability proof from [15], which shows UGAS and ULES of the origin of (46b) implies that inequality (58) holds, i.e. Condition 2c holds.

Remark 12: Note however, that (58) does not imply that the origin of (46b) is UGAS because (58) only holds for the existence of the solutions [22].

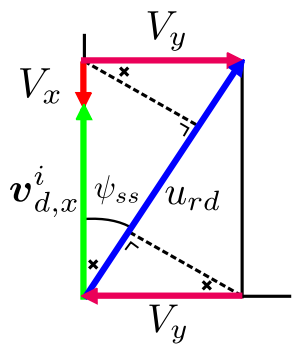

Fig. 3. Steady-state velocity assignment

Condition 2) can now be verified using Theorem A.1:

Proposition 1: Given that the conditions of Theorem 1 are satisfied, then the solutions of (46) are uniformly globally bounded.

TABLE I
SIMULATION PARAMETERS.

Variable	Value	Unit	Variable	Value	Unit
Δ	350	m	σ	1.5	-
$V_{x,1}$	-1.1028	m/s	$V_{y,1}$	0.8854	m/s
$V_{x,2}$	-1.1028	m/s	$V_{y,2}$	0.4427	m/s
$V_{x,3}$	-0.8822	m/s	$V_{y,3}$	0.1771	m/s
D_2	200	m	D_3	-200	m
d_{12}	-200	m	d_{13}	-100	m
$\boldsymbol{v}^i_{d,x}$	5	m/s	a	0.5	m/s

Proof: We use

$$\alpha_5(|\boldsymbol{\phi}|) \triangleq C_1 \tag{61}$$

$$\alpha_5'(|\boldsymbol{\zeta}|) \triangleq \alpha_4'(|\boldsymbol{\zeta}|) \tag{62}$$

with C_1 from (41). It can then be verified that Theorem A.1 in Appendix II holds, which implies that the solutions of (46) are uniformly globally bounded. ∎

Theorem 2: Consider a formation of n vessels described by (4). Suppose that u_d is continuously differentiable, Assumptions 1-5 are satisfied, and the communication graph contains at least one globally reachable vertex. If the look-ahead distance Δ and the integral gain σ satisfy the conditions

$$\Delta_j > \frac{|X_{\max_j}|}{|Y_{\min_j}|}\left[\frac{5}{4}\frac{U_{\max_j}+V_{\max_j}+\sigma_j}{U_{\min_j}-V_{\max_j}-\sigma_j}+1\right], \tag{63}$$

$$0 < \sigma_j < U_{\min_j} - V_{\max_j}, \tag{64}$$

for $j = 1, \ldots, n$, then the origin of (46 is UGAS.

Proof: It is shown that both Condition 1 and Proposition 1 hold and hence we can invoke [22, Proposition 2], given as Proposition A.1 in Appendix II, for system (46). ∎

This implies that the control goals (5)-(8) are achieved and thus the proof of Theorem 1 is complete.

V. CASE STUDY

This case study considers three vessels, each vessel is disturbed by a different current. The simulation parameters are given in Table I. The minimum desired velocity is saturated to $u_d = 3$ [m/s] to assure that (64) is satisfied. The initial position for the vessels is given by

$$\begin{bmatrix} x_{1o} \\ y_{1o} \\ \psi_{1o} \end{bmatrix} = \begin{bmatrix} 0 \\ -1000 \\ 180 \end{bmatrix}, \begin{bmatrix} x_{2o} \\ y_{2o} \\ \psi_{2o} \end{bmatrix} = \begin{bmatrix} 0 \\ 500 \\ 90 \end{bmatrix}, \begin{bmatrix} x_{3o} \\ y_{3o} \\ \psi_{3o} \end{bmatrix} = \begin{bmatrix} 0 \\ -500 \\ -90 \end{bmatrix}.$$

The communication protocol is such that vessel 1 sends its position to vessel 2 and 3 while only vessel 3 sends its position back to vessel 1. The planar movement can be seen in Figure

The ship trajectories with the proposed control approach can be seen in Figure 4. From Figure 4 it can be seen that the ships converge to their respective paths and that the desired formation is achieved.

The coupling between yaw angle and speed can be seen when considering Figure 5 and Figure 6. In the first hundred seconds of the simulation, when the yaw controllers are converging to their desired value, the relative surge speed for two of the ships rises fast only to decrease again when the yaw controllers have converged. Moreover, since each vessel is disturbed by a different current the steady-state values for the yaw angles and surge velocity are different for each ship.

The path following error and formation errors can be seen in Figure 7 and Figure 8 respectively. From these figures it can be seen that the path following errors and the formation errors converge to zero.

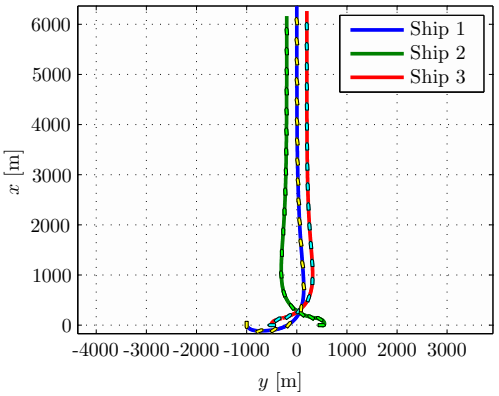

Fig. 4. Ship trajectories in 2-D space

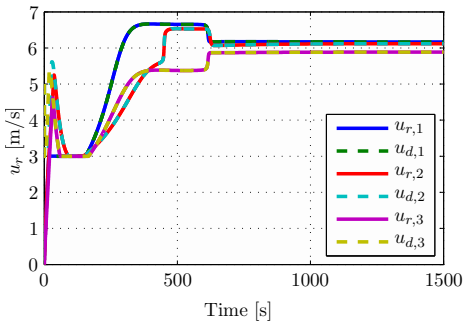

Fig. 5. Surge speed assignment

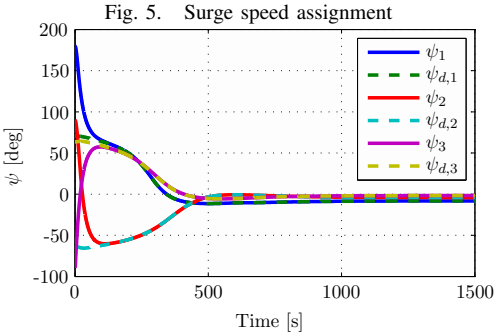

Fig. 6. Yaw angle assignment

VI. CONCLUSIONS

In this paper straight-line path following with disturbance rejection for inhomogeneous formations with underactuated agents has been considered. The agents under consideration were represented by a 3-DOF manoeuvring model that was disturbed by an unknown ocean current. Path following in formation has been achieved by employing integral LOS guidance to reject the disturbance and a decentralised formation control law that achieves synchronisation by letting each vessel utilise locally available information only. The origin of the closed loop error dynamics consisting of the path following error dynamics and formation error dynamics is shown to be UGAS using theory for nonlinear cascaded systems which allow a feedback-interconnected system to be analysed as a cascade under certain conditions.

APPENDIX I
FUNCTION DEFINITIONS

The functions F_{u_r}, $X(u_r)$, $Y(u_r)$, and F_r are given by:

$$F_{u_r} \triangleq \frac{1}{m_{11}}(m_{22}v_r + m_{23}r)r, \tag{65}$$

$$X(u_r) \triangleq \frac{m_{23}^2 - m_{11}m_{33}}{m_{22}m_{33}-m_{23}^2}u_r + \frac{d_{33}m_{23}-d_{23}m_{33}}{m_{22}m_{33}-m_{23}^2}, \tag{66}$$

$$Y(u_r) \triangleq \frac{(m_{22}-m_{11})m_{23}}{m_{22}m_{33}-m_{23}^2}u_r - \frac{d_{22}m_{33}-d_{32}m_{23}}{m_{22}m_{33}-m_{23}^2}, \tag{67}$$

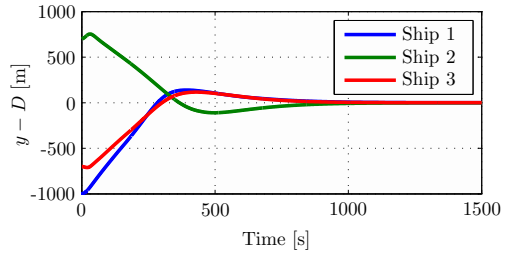

Fig. 7. Path following errors

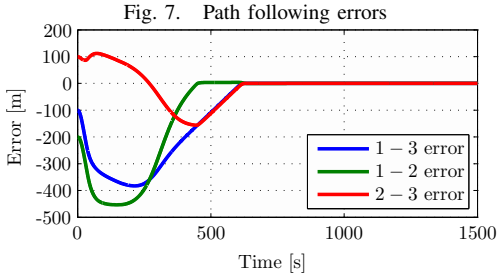

Fig. 8. Formation errors

$$F_r(u_r, v_r, r) \triangleq \frac{m_{23}d_{22} - m_{22}(d_{32} + (m_{22} - m_{11})u_r)}{m_{22}m_{33} - m_{23}^2} v_r + \frac{m_{23}(d_{23} + m_{11}u_r) - m_{22}(d_{33} + m_{23}u_r)}{m_{22}m_{33} - m_{23}^2} r. \tag{68}$$

Functions $\boldsymbol{h}_y \triangleq [h_{y_1}, h_{y_2}, h_{y_3}]^T$ and $\boldsymbol{h}_{v_r} \triangleq [h_{v_{r1}}, h_{v_{r2}}, h_{v_{r3}}]^T$ are given by:

$$\begin{aligned} h_{y,1} &= \sin(\tilde{\psi} + \psi_d),\ h_{y,3} = 0, \\ h_{y,2} &= u_c \left[\frac{\sin(\tilde{\psi})}{\tilde{\psi}} \cos(\psi_d) + \frac{\cos(\tilde{\psi}) - 1}{\tilde{\psi}} \sin(\psi_d) \right] \\ &\quad + v_r \left[\frac{\cos(\tilde{\psi}) - 1}{\tilde{\psi}} \cos(\psi_d) - \frac{\sin(\tilde{\psi})}{\tilde{\psi}} \sin(\psi_d) \right], \end{aligned} \tag{69}$$

$$\begin{aligned} h_{v_r,1} &= \frac{X(\tilde{u}_r + u_c) - X^{u_c}}{\tilde{u}_r} \gamma(y_{\text{int}}, y, v_r) + v_r \frac{Y(\tilde{u}_r + u_c) - Y^{u_c}}{\tilde{u}_r}, \\ h_{v_r,2} &= 0, \qquad h_{v_r,3} = X(\tilde{u}_r - u_c), \end{aligned} \tag{70}$$

with $\gamma(y_{\text{int}}, y, v_r)$ defined as:

$$\gamma(y_{\text{int}}, y, v_r) \triangleq \frac{\Delta(u_c(y + \sigma y_{\text{int}}^{\text{eq}}) - \Delta v_r)}{((e_2 + \sigma y_{\text{int}}^{\text{eq}})^2 + \Delta^2)^{3/2}} - \frac{\Delta V_y}{(e_2 + \sigma y_{\text{int}}^{\text{eq}})^2 + \Delta^2} - \frac{\sigma\Delta}{((e_2 + \sigma y_{\text{int}}^{\text{eq}})^2 + \Delta^2)^2} (y - D_j). \tag{71}$$

Appendix II
Reference Theorems

This appendix presents Theorem 2 and Proposition 2 from [22] which are used in the stability proof of the cloased-loop system in Section IV.

Theorem A.1 ([22, Theorem 2]): Consider system (47) under the following conditions:

1) Condition 2a, 2b, and 2c hold;
2) there exist $\alpha_5, \alpha_5' \in \mathcal{K}$ such that

$$|[L_g V]| \leq \alpha_5(|x_1|)\alpha_5'(|x_2|) \tag{72}$$

and for each $r > 0$ there exist $\lambda_r, \eta_r > 0$ such that

$$t \geq 0,\ |x_1| \geq \eta_r \implies \alpha_5(|x_1|) \leq \lambda_r W(x_1) \tag{73}$$

Then, the solutions of (47) are uniformly globally bounded.

Proposition A.1 ([22, Proposition 2]): Under Condition 1 and the conditions of Theorem A.1 the origin of (47) is UGAS.

References

[1] H. Bai, M. Arcak, and J. T. Wen, *Cooperative control design*. Springer, 2011, vol. 89.

[2] V. Kumar, N. Leonard, and A. Morse, *Cooperative Control*. Springer-Verlag, 2005.

[3] K. Y. Pettersen, J. T. Gravdahl, and H. Nijmeijer, *Group coordination and cooperative control*. Springer Berlin, 2006, vol. 336.

[4] K. D. Do and J. Pan, "Nonlinear formation control of unicycle-type mobile robots," *Robotics and Autonomous Systems*, vol. 55, no. 3, pp. 191–204, 2007.

[5] E. I. Grøtli, A. Chaillet, E. Panteley, and J. T. Gravdahl, "Optimal controller gain tuning for robust stability of spacecraft formation," in *Informatics in Control, Automation and Robotics*. Springer, 2011, pp. 335–347.

[6] J. Almeida, C. Silvestre, and A. Pascoal, "Cooperative control of multiple surface vessels in the presence of ocean currents and parametric model uncertainty," *International Journal of Robust and Nonlinear Control*, vol. 20, no. 14, pp. 1549–1565, 2010.

[7] R. Ghabcheloo, A. P. Aguiar, A. Pascoal, C. Silvestre, I. Kaminer, and J. Hespanha, "Coordinated path-following in the presence of communication losses and time delays," *SIAM Journal on Control and Optimization*, vol. 48, no. 1, pp. 234–265, 2009.

[8] E. Børhaug, A. Pavlov, E. Panteley, and K. Y. Pettersen, "Straight line path following for formations of underactuated marine surface vehicles," *IEEE Transactions on Control Systems Technology*, vol. 19, no. 3, pp. 493–506, 2011.

[9] Y. Y. Chen and Y. P. Tian, "Formation tracking and attitude synchronization control of underactuated ships along closed orbits," *International Journal of Robust and Nonlinear Control*, 2014, DOI:10.1002.

[10] I.-A. F. Ihle, J. Jouffroy, and T. I. Fossen, "Formation control of marine surface craft: A lagrangian approach," *IEEE Journal of Oceanic Engineering*, vol. 31, no. 4, pp. 922–934, 2006.

[11] Z. Peng, D. Wang, Z. Chen, X. Hu, and W. Lan, "Adaptive dynamic surface control for formations of autonomous surface vehicles with uncertain dynamics," *IEEE Transactions on Control Systems Technology*, vol. 21, no. 2, pp. 513–520, 2013.

[12] M. Burger, A. Pavlov, E. Borhaug, and K. Y. Pettersen, "Straight line path following for formations of underactuated surface vessels under influence of constant ocean currents," in *Proc. of the American Control Conference*, 2009, pp. 3065–3070.

[13] E. Børhaug, A. Pavlov, and K. Y. Pettersen, "Integral los control for path following of underactuated marine surface vessels in the presence of ocean currents," in *Proc. of the 47th IEEE Conference on Decision and Control*, 2008, pp. 4984–4991.

[14] D. J. W. Belleter and K. Y. Pettersen, "Path following for formations of underactuated marine vessels under influence of constant ocean currents," in *Proceedings of the 53th IEEE Conference on Decision and Control, Los Angeles, USA, Dec. 15-17*, 2014, pp. 4521–4528.

[15] W. Caharija, M. Candeloro, K. Y. Pettersen, and A. J. Sørensen, "Relative velocity control and integral los for path following of underactuated surface vessels," in *Proc. of the 9th IFAC Conference on Manoeuvring and Control of Marine Craft*, 2012.

[16] D. J. W. Belleter and K. Y. Pettersen, "Underactuated leader-follower synchronisation for multi-agent systems with rejection of unknown disturbances," in *American Control Conference, Chicago, USA*, 2015.

[17] T. I. Fossen, *Handbook of Marine Craft Hydrodynamics and Motion Control*. Wiley, 2011.

[18] E. Fredriksen and K. Y. Pettersen, "Global κ-exponential way-point maneuvering of ships: Theory and experiments," *Automatica*, vol. 42, no. 4, pp. 677–687, 2006.

[19] E. Kyrkjebø, "Motion coordination of mechanical systems," Ph.D. dissertation, Norwegian University of Science and Technology, 2007.

[20] M. Mesbahi and M. Egerstedt, *Graph theoretic methods in multiagent networks*. Princeton University Press, 2010.

[21] C. Godcil and G. Royle, "Algebraic graph theory," *Ser. Springer Graduate Texts in Mathematics*, vol. 207, 2001.

[22] A. Loría, "From feedback to cascade-interconnected systems: Breaking the loop," in *Decision and Control, 2008. CDC 2008. 47th IEEE Conference on*. IEEE, 2008, pp. 4109–4114.